Title
Generalized Lévy walks and the role of chemokines in migration of effector CD8+ T cells

Permalink
https://escholarship.org/uc/item/8ws3525x

Journal
Nature, 486(7404)

ISSN
0028-0836

Authors
Harris, Tajie H
Banigan, Edward J
Christian, David A
et al.

Publication Date
2012-06-01

DOI
10.1038/nature11098

Peer reviewed

Generalized Lévy walks and the role of chemokines in migration of effector CD8+ T cells

Tajie H. Harris[1], **Edward J. Banigan**[2], **David A. Christian**[1], **Christoph Konradt**[1], **Elia D. Tait Wojno**[1], **Kazumi Norose**[3], **Emma H. Wilson**[4], **Beena John**[1], **Wolfgang Weninger**[5], **Andrew D. Luster**[6], **Andrea J. Liu**[2], and **Christopher A. Hunter**[1]

[1]Department of Pathobiology, School of Veterinary Medicine, University of Pennsylvania, 380 S. University Ave., Philadelphia, PA 19104, USA

[2]Department of Physics and Astronomy, School of Arts and Sciences, University of Pennsylvania, 209 S. 33rd St., Philadelphia, PA 19104, USA

[3]Department of Infection and Host Defense, Graduate School of Medicine, Chiba University 1-8-1, Inohana, Chuo-ku, Chiba, 260-8670, Japan

[4]Division of Biomedical Sciences, University of California-Riverside, Riverside, CA 92521, USA

[5]The Centenary Institute, Newtown, NSW 2042 and Discipline of Dermatology, Sydney Medical School, Sydney, NSW, Australia

[6]Center for Immunology and Inflammatory Diseases, Division of Rheumatology, Allergy and Immunology, Massachusetts General Hospital, Building 149, 13th Street, Room 8301, Charlestown, MA 02129, USA

Abstract

Chemokines play a central role in regulating processes essential to the immune function of T cells[1-3], such as their migration within lymphoid tissues and targeting of pathogens in sites of inflammation. Here we track T cells using multi-photon microscopy to demonstrate that the chemokine CXCL10 enhances the ability of CD8+ T cells to control the pathogen *T. gondii* in the brains of chronically infected mice. This chemokine boosts T cell function in two different ways: it maintains the effector T cell population in the brain and speeds up the average migration speed without changing the nature of the walk statistics. Remarkably, these statistics are not Brownian; rather, CD8+ T cell motility in the brain is well described by a generalized Lévy walk. According to our model, this surprising feature enables T cells to find rare targets with more than an order of magnitude more efficiency than Brownian random walkers. Thus, CD8+ T cell behavior is similar

---

Correspondence and requests for materials should be addressed to A.J.L. (ajliu@physics.upenn.edu) and C.A.H. (chunter@vet.upenn.edu)..

to Lévy strategies reported in organisms ranging from mussels to marine predators and monkeys[4-10], and CXCL10 aids T cells in shortening the average time to find rare targets.

Toxoplasma gondii is an opportunistic pathogen that causes encephalitis in patients with acquired defects in T cell function[11]. Multiple studies have established that resistance to this parasite in the central nervous system (CNS) relies on T cell production of IFN-γ and cytotoxic T cells, but little is known about the factors that regulate the behavior of effector T cells at this site[12-14]. In order to understand the role of chemokines in directing T cells to regions of infection during toxoplasmic encephalitis (TE), real-time PCR was performed to assess changes in chemokine receptor expression in the brains of infected mice (Supplementary Fig. 1a). Notably, mRNA transcripts for CXCR3, a receptor expressed by activated and memory T cells, and associated with Th1 type responses[15,16] and its ligands, CXCL9 and CXCL10, were highly expressed during TE (Fig. 1a). Previous studies have demonstrated extensive production of *cxcl10* mRNA by activated astrocytes during TE[17]. Analysis of lymphocytes isolated from the brains of mice infected with ovalbumin-expressing parasites (Pru^{OVA}) revealed that CD8$^+$ T cells, including those specific for ovalbumin, express CXCR3 (Fig. 1b) and migrate towards CXCL10 *ex vivo* (Fig. 1c). Thus, parasite-specific CD8$^+$ T cells present in the CNS during TE are responsive to CXCR3 ligands.

While CXCL10 is required for resistance to acute *T. gondii* infection[18], little is known about how this molecule affects T cell responses during chronic TE. Therefore, we treated chronically infected mice with anti-CXCL10 antibodies. One week later, mononuclear cells from the brain were isolated, and T cells were quantified by flow cytometry. Anti-CXCL10 treatment led to a 40% decrease in the number of CD8$^+$ T cells (Fig. 2a, *p*=0.04) and an increase in parasite burden (Fig. 2b, *p*=0.04). Immunohistochemical staining for *T. gondii* revealed latent cyst forms in control mice (Fig. 2c), while regions of active parasite replication were observed in the brains of anti-CXCL10-treated mice (Fig. 2d). To address the role of CXCL10 in the recruitment and maintenance of antigen-specific T cells in the CNS, we used an adoptive transfer system. *In vitro* activated OVA-specific OT-I cells were transferred to mice chronically infected with Pru^{OVA}, resulting in the migration and accumulation of these cells within the CNS[19]. When OT-I T cells were transferred to chronically infected wildtype C57BL/6 or CXCL10-deficient mice, knockout mice had 60% fewer transferred cells in the brain in comparison to wildtype mice, while equivalent numbers were recovered from the spleen and lymph node in both groups (Supplementary Fig. 1b-c). Similar results were obtained when CXCR3$^{-/-}$ and WT OT-I cells were transferred to wildtype mice chronically infected with Pru^{OVA} (Supplementary Fig. 1d-e).

These studies show that CXCL10 and CXCR3 are required for optimal recruitment and/or retention of antigen-specific CD8$^+$ T cells in the CNS during TE. To determine whether CXCL10 and chemokine signals also affect the *migration* of CD8$^+$ T cells once they enter the CNS, we used multi-photon (MP) imaging to track GFP-expressing OT-I T cells (OT-I^{GFP}) in explant brain following short-term anti-CXCL10 treatment (Supplementary Movies 1-2). In addition, chemokine signals were inhibited using pertussis toxin, an inhibitor of Gα$_i$ signaling[2] (Supplementary Movie 3). We imaged cells for 10-30 minutes since cells migrate

out of the field of view during longer imaging periods, biasing our sample towards cells that are less motile. Analysis of the cell tracks (Fig. 2e-g) revealed that anti-CXCL10 treatment reduced the average cell velocity 23% from 6.35 μm/min in control treated mice to 4.88 μm/min (Fig. 2h), while pertussis toxin reduced the track velocity 46% to 3.45 μm/min. Plots of individual cell tracks demonstrate that cells cover less area over a 10-minute time span in the absence of CXCL10 or when treated with pertussis toxin (Fig. 2i-k).

We performed a standard analysis to quantitatively determine how chemokines affect the migratory behavior of CD8$^+$ T cells by extracting the motility coefficient (Supplementary Fig. 2). This analysis implicitly assumes a Brownian walk since the motility coefficient is extracted from the slope of the best linear fit to the mean-squared displacement (MSD), $\langle r^2(t) \rangle$, as a function of time, t[20]. However, when we plot the MSD on a log-log plot, it grows with time approximately as t^α, with $\alpha \approx 1.4$ (Fig. 3a). This finding suggests that the T cell tracks are not Brownian walks.

To determine the type of random walk that best describes the migration data, we focused not only on the behavior of the MSD, but also on the shape of the tracks, the probability distribution, $P(\overrightarrow{r}(t))$, of cell displacements, $\overrightarrow{r}(t)$, as a function of the time interval, t, and the decay of normalized displacement correlations,

$\langle K(\tau, t) \rangle = \langle r(0,t) \cdot r(\tau, \tau+t) \rangle / \langle r^2(0,0) \rangle$, as a function of , τ where $\overrightarrow{r}(\tau, \tau+t)$ is the displacement between times τ and $\tau + t$. Together, these properties provide a more complete description of the walk statistics than the MSD alone, and therefore provide far more constraints that must be satisfied by a candidate random walk model. First, by analyzing statistics of the cell trajectory shapes, we established that CD8$^+$ T cells do not exhibit directional migration on the time and length scales relevant to this experiment (see Supplementary Fig. 3 and Supplementary Discussion). To analyze the displacement distribution, we introduced a time-dependent variable, $\zeta(t)$, to scale the cell displacements. For Brownian walks, the distribution, $\widetilde{P}\rho$, of *scaled* displacements, $\rho(t) \equiv \tilde{r}(t)$ should be

Gaussian, $\widetilde{P}(\rho) = \dfrac{1}{\sqrt{2\pi}} e^{-\rho^2/2}$, and the scale factor, $\zeta(t)$, should be the root-mean-squared displacement (RMSD). However, for the migrating CD8$^+$ T cells, the distribution $P(\tilde{\rho})$ is not Gaussian (Fig. 3b, inset); the probability of large displacements is much larger than expected at all times studied. Remarkably, $P(\tilde{\rho})$ has the same shape at all times, indicating that the tracks are also not well described by persistent random walks. Moreover, the scale factor obeys $\zeta(t) \sim t^\gamma$ with $\gamma = 0.63$, not $\gamma = 1/2$, as expected for Brownian walks, (Fig. 3c), and clearly differs from the RMSD (Supplementary Fig. 4) at all times studied. Finally, the displacement correlations do not decay exponentially in time, as for Brownian walks (inset to Fig. 3c). Thus, Brownian walks do not describe effector T cell migration during TE.

Based on these walk statistics, we considered several variations of Lévy walks (see Supplementary Table 1, Supplementary Fig. 5, and Supplementary Discussion). We find that, consistent with early observations of runs and pauses in lymphocytes[21], T cell migration is well-described by the following model of a generalized Lévy walk[22]. Walkers make straight runs at fixed velocity in random directions over distances chosen randomly from a Lévy distribution, $L_\mu(\ell) \sim \ell^{-\mu}$, with $\mu_{run} = 2.15$. After each run, a walker pauses for a

time whose duration is drawn from a Lévy distribution with $\mu_{pause}=1.7$. The values of the exponents μ_{run} and μ_{pause} were determined from a maximum likelihood analysis[23] (see Supplementary Discussion). The model captures quantitatively the observed displacement distributions at different times (Fig. 3b), the time evolution of the MSD and scale factor (Fig. 3a and 3c, respectively), the decay of displacement correlations (inset to Fig. 3c), and qualitative features of cell tracks (Supplementary Fig. 6). An Akaike weight analysis[24] indicates that the generalized Lévy walk model does a better job of fitting the displacement distributions than any of the other models we have considered, including, for example, bimodal correlated random walks[25] (see Supplementary Table 1, Supplementary Fig. 5, and Supplementary Discussion). The generalized Lévy walk model is consistent with our data over 30 minutes (Supplementary Figure 7), and also describes the behavior of polyclonal CD8+ T cells, transgenic LCMV-specific CD8+ T cells migrating in the absence of cognate antigen, and CD8+ T cells migrating in the brains of live animals (Supplementary Fig. 8).

In the absence of CXCL10 or signals through $G\alpha_i$-coupled receptors, the migration statistics for CD8+ T cells are well described by the same generalized Lévy walk model, characterized by $\mu_{run}=2.15$ and $\mu_{pause}=1.7$ (Supplementary Figs. 6 and 8), as for control cells, but with either a reduced instantaneous speed during runs or longer pauses. Therefore, the chemokine CXCL10 and signals through $G\alpha_i$-coupled receptors speed up migration without otherwise changing the walk statistics. This result, together with the fact that we find no evidence of directed migration over the time scales investigated (see Supplementary Discussion), suggests a chemokinetic role for CXCL10 during TE.

Previous studies have demonstrated that neutrophil or CD8+ T cell control of bacteria or tumor cells, respectively, can be understood by a rate equation in which the killing of targets is modeled as a collision-based process[26,27]. We incorporated the generalized Lévy walk statistics into a similar model to predict the time required to find rare target cells. In our model, we placed N generalized Lévy walkers randomly in a sphere of volume V with a target of radius a at the origin (Supplementary Fig. 9a). We find that cells migrating by generalized Lévy walks are significantly more efficient in finding target cells than those performing Brownian walks (Fig. 4 and Supplementary Fig. 9b-c). Here, the efficiency is the inverse of the sum of the displacements of all the walkers at the instant when the first walker reaches the target[28]. In the absence of CXCL10 or signals through $G\alpha_i$-coupled receptors, our model predicts that for estimated values of a, V, and N, the capture time for a CD8+ T cell to reach the target is increased by factors of 1.9 or 3.0, respectively, in comparison to the control setting (see Supplementary Fig. 9d-f and Supplementary Discussion). These results suggest that the ability of CD8+ T cells to find and control *T. gondii*-infected targets in the CNS is aided by a generalized Lévy walk search strategy, and the capture time is shortened by CXCL10, and likely by other chemokines as well. We emphasize that the generalized Lévy walk is not necessarily an optimal search strategy, and a model with $\mu_{run}=2.0$ would be more efficient according to this definition[28]. Moreover, the efficiency is highly dependent on details of the environment and search/capture process[29] that are not presently known, so determination of the optimal search strategy remains an open question.

Lévy search strategies may be used by diverse species, including microzooplankton, fruit flies, honey bees, mussels, predatory fish, sea turtles, penguins, and spider monkeys[4-10]. Our

results show that a generalization of this search strategy appears to be relevant, at the single cell level, to the ability of effector cells to find rare targets. In addition, our findings provide a novel insight into the role of CXCL10 as a chemokine that specifically influences the capture time for CD8^{+} T cells to find infected targets during toxoplasmic encephalitis. Altogether, our findings raise several fundamental questions as to whether lymphocytes execute generalized Lévy walks in other environments, how activation status affects walk statistics, and whether the pauses suggested by our model arise from factors internal to the cell or from interactions of the cells with their external environment.

Methods Summary

T. gondii infection was established by intraperitoneal injection of ovalbumin-expressing Prugnaud strain (Pru[OVA]) tachyzoites. Real time PCR was performed for chemokine receptor expression and *T. gondii* DNA quantification. Brain mononuclear cells were stained with fluorescently conjugated antibodies for flow cytometric analysis. OT-I cells were activated *in vitro* and transferred to recipient mice. Mice were treated with four doses of 100 μg of anti-CXCL10 for week-long depletion studies or 300 μg 18 hours prior to imaging studies. Pertussis toxin was administered at 400 μg/kg six hours before imaging. For MP microscopy, explant brain was imaged using a Leica SP5 2-photon microscopy system. Cell tracking was performed using Volocity software. In order to create displacement histograms without binning artifacts[30] (Supplementary Tables 2-3), a constant number of displacements were placed in each bin. Various statistical methods were applied to test the validity of the generalized Lévy walk model (see Fig. 3, Supplementary Figs. 3, 5, 7, 8, 10, Supplementary Table 1, and Supplementary Discussion). Brownian dynamics-like simulations were performed to simulate the general behavior and searching capability of Gaussian ("random") and Lévy walkers (see Supplementary Discussion). *N* searchers were placed in a spherical volume of radius *b,* and they moved stochastically until finding the target of radius *a*, which was stationary at the center of the sphere. During random walks, searchers moved $\sqrt{6D\Delta t}$ = 0.1μm in the *x-, y-,* or *z*-direction each time step; here *D* is the motility coefficient and Δt is the time step. In Lévy walk simulations, a direction for a run was chosen at random, and run lengths were drawn from a Lévy distribution with exponent μ_{run}=2.15. Searchers moved a distance $v\Delta t$ each time step until the run was completed. After each run, the walker paused for a time drawn from Lévy distribution with μ_{pause}=1.7.

Supplementary Material

Refer to Web version on PubMed Central for supplementary material.

Acknowledgements

METHODS

Mice, parasites, and antibody

C57BL/6, CXCL10-deficient, C57BL/6 Thy1.1, and OT-I transgenic, and mice expressing DsRed under the actin promoter mice were purchased from The Jackson Laboratory (Bar Harbor, ME). DPE[GFP] mice were originally obtained from Ulrich von Andrian (Harvard University, Boston, MA) and crossed with OT-I mice. CXCR3^{-/-} mice were originally obtained from Craig Gerard (Harvard University) and crossed to OT-I mice. DsRed P14 mice were the generous gift of Dr. Steve Reiner (University of Pennsylvania, Philadelphia, PA). All procedures were performed in accordance to the guidelines of the University of Pennsylvania Institutional Animal Care and Use Committee. Ovalbumin-expressing Prugnaud strain parasites (Pru[OVA]) were generated and maintained as previously described[31,32]. Female mice were infected with 10^4 tachyzoites in 200 μl PBS i.p. Hamster anti-CXCL10 antibodies (clone 1F11, generated as previously described[20]) and normal hamster IgG (Jackson Immunoresearch, West Grove, PA) were administered i.p. in PBS. Pertussis toxin (400 μg/kg, Sigma) was administered i.p. for six hours prior to imaging experiments.

Real-time PCR

For the analysis of gene expression, brain tissue was placed in Trizol (Invitrogen, Carlsbad, CA) and mRNA was extracted as instructed by the manufacturer. Purified RNA was treated with DNAse I to eliminate any contamination with genomic DNA (Promega, Madison, WI). cDNA was generated using Superscript II reverse transcriptase (Invitrogen). Real-time PCR was performed using Quantitect primers (Qiagen, Germantown, MD) specific for *ccr1*, *ccr3-10*, *cxcr1-6*, *cxc3cr1*, *xcr1*, *cxcl9*, and *cxcl10* or primers for *ccr2* (forward 5-CACACCCTGTTTCGCTGTA-3 and reverse 5-TGCATGGCCTGGTCTAAGTG-3) and normalized to *hprt* (Qiagen). To measure the amount of parasite DNA in the brain, real-time PCR was utilized as previously described[33]. PCR was performed using Power SYBRr Green PCR Master Mix and a 7500 Fast Real-Time PCR System (Applied Biosystems, Warrington, UK).

Flow cytometry

Single cell suspensions were generated from spleen and lymph node by macerating the tissues through a 70 μm nylon mesh filter (BD Falcon, Bedford, MA). Spleen samples were subjected to hypotonic red blood cell lysis. Brain mononuclear cells (BMNCs) were isolated as previously described[33]. Briefly, perfused brains were homogenized and digested with collagenase/dispase and DNase (Roche). Following the digestion, the cells were purified using a percoll gradient. For flow cytometry, $1\text{-}2 \times 10^6$ cells were incubated with 0.1 μg/ml 24G2 antibody prior to surface staining with PE conjugated-K^b-SIINFEKL tetramer reagent (Benton-Dickinson), CXCR3-APC (R&D Systems, Minneapolis, MN), Thy1.2-PECy7, CD4-FITC, CD8-PerCpCy5.5, CD8-eFlour780, CD45-APC, CD45.1-PerCpCy5.5 (eBioscience). All flow cytometry was performed on a FACsCanto using FACsDIVA 6.0

software (BD Biosciences, San Jose, CA). Analysis was performed using FloJo software (Treestar Inc., Ashland, OR).

Ex vivo chemotaxis assay

Purified splenocytes and brain mononuclear cells were rested for one hour at in complete RPMI prior to the chemotaxis assay. Cells were resuspended in chemotaxis assay medium (RPMI, 0.5% BSA, 25 mM HEPES). Cells (2×10^5) were placed in the upper chamber of a 6.5 mm transwell insert with a 5 μm pore size membrane (Corning, Lowell, MA). CXCL9, CXCL10, or CXCL11 (R&D Systems) was present in the lower chamber at various concentrations (0-300 nM). Following 90 minutes, CD45$^+$ cells that migrated through the filter were enumerated using fluorescent beads (Polysciences, Warrington, PA) and phenotyped by flow cytometry.

In vitro activation of T cells

OT-I cells were expanded from the spleen and lymph nodes of OT-I transgenic mice. Lymphocytes were cultured with 500 μg/ml chicken ovalbumin protein (Worthington, Lakewood, NJ) for 24 hours. The cells were washed and rested for 2 days and received 200 U/ml IL-2 on days 4 and 6 of culture. On day 7 of culture, cells were washed in PBS and enumerated. 2-5 $\times 10^6$ cells were transferred i.v. For polyclonal expansion of T cells, CD8$^+$ T cells were enriched from the lymph nodes and spleens of C57BL/6, DsRed, DsRed P14, or GFP OT-I mice by magnetic separation (Miltenyi Biotech, Boston, MA). T cells were plated in the presence of platebound anti-CD3 (1 μg/ml, eBioscience) and anti-CD28 (3 μg/ml, eBioscience), 200 U/ml IL-2, and anti-IL-4 (1 μg/ml, NCI Preclinical Repository). The cells were split and supplemented with 200 U/ml IL-2 on day 2 of culture. On day 4 of culture, cells were washed and 10-20 $\times 10^6$ T cells were transferred i.v.

Immunohistochemistry

For immunohistochemistry, organs were embedded in OCT and flash frozen. Anti-CD8 (5 μg/ml) (eBioscience, San Diego, CA), anti-Me49 (generous gift from Dr. F. Araujo, Palo Alto Medical Foundation, Palo Alto, CA), anti-rabbit Alexa 488 (Invitrogen), and anti-rat Cy3 (Jackson Immunoresearch) were used for fluorescence staining. DAPI (Invitrogen) was used to visualize nuclei. Images were captured using standard fluorescence microscopy using a Nikon Eclipse E600 microscope (Melville, NY) equipped with a Photometrics Cool Snap EZ CCD camera (Tucson, AZ). Nikon NIS Elements software was used to capture and overlay images.

Multi-photon imaging

Mice were sacrificed by CO_2 asphyxiation and the brains were removed immediately, with minimal mechanical disruption and placed in heated chamber where specimens were constantly perfused with warmed (37°C), oxygenated media (phenol-red free RPMI 1640 supplemented with 10% FBS, Gibco). The temperature in the imaging chamber was maintained at 37°C using heating elements and monitored using a temperature control probe. For the imaging of live mice, mice were anesthetized and cells were imaged through

thinned skull. The core temperature of the mice was monitored and maintained at 37°C. Imaging was done using a Leica SP5 2-photon microscope system (Leica Microsystems, Mannheim, Germany) equipped with a picosecond or femtosecond laser (Coherent Inc., Santa Clara, CA) GFP was excited using laser light of 920 nm. Images were obtained using a 20X water-dipping lens. Four-dimensional imaging data was collected by obtaining images from the x-, y-, and z-planes, with a z- thickness of 28 μm and step size of 4 μm to allow for the capture of a complete z-series every 22 seconds. This was carried out for approximately 10 minutes, which was the typical time elapsed before a significant number of cells had left the field of view. The resulting images were analyzed with Volocity software to obtain individual cell track data (PerkinElmer, Waltham, MA).

References

1. Bromley SK, Mempel TR, Luster AD. Orchestrating the orchestrators: chemokines in control of T cell traffic. Nat Immunol. 2008; 9:970–980. [PubMed: 18711434]

2. Cyster JG. Chemokines, sphingosine-1-phosphate, and cell migration in secondary lymphoid organs. Annu Rev Immunol. 2005; 23:127–159. [PubMed: 15771568]

3. Ebert LM, Schaerli P, Moser B. Chemokine-mediated control of T cell traffic in lymphoid and peripheral tissues. Mol Immunol. 2005; 42:799–809. [PubMed: 15829268]

4. Bartumeus F, Peters F, Pueyo S, Marrase C, Catalan J. Helical Levy walks: adjusting searching statistics to resource availability in microzooplankton. Proc Natl Acad Sci U S A. 2003; 100:12771–12775. [PubMed: 14566048]

5. Reynolds AM, Frye MA. Free-flight odor tracking in Drosophila is consistent with an optimal intermittent scale-free search. PLoS One. 2007; 2:e354. [PubMed: 17406678]

6. Humphries NE, et al. Environmental context explains Levy and Brownian movement patterns of marine predators. Nature. 465:1066–1069. [PubMed: 20531470]

7. de Jager M, Weissing FJ, Herman PMJ, Nolet BA, van de Koppel J. Levy Walks Evolve Through Interaction Between Movement and Environmental Complexity. Science. 2011; 332:1551–1553. [PubMed: 21700872]

8. Boyer D, et al. Scale-free foraging by primates emerges from their interaction with a complex environment. Proc Biol Sci. 2006; 273:1743–1750. [PubMed: 16790406]

9. Reynolds AM, et al. Displaced honey bees perform optimal scale-free search flights. Ecology. 2007; 88:1955–1961. [PubMed: 17824426]

10. Sims DW, et al. Scaling laws of marine predator search behaviour. Nature. 2008; 451:1098–1102. doi:10.1038/nature06518. [PubMed: 18305542]

11. Montoya JG, Liesenfeld O. Toxoplasmosis. Lancet. 2004; 363:1965–1976. doi:10.1016/S0140-6736(04)16412-X. [PubMed: 15194258]

12. Denkers EY, et al. Perforin-mediated cytolysis plays a limited role in host resistance to Toxoplasma gondii. J Immunol. 1997; 159:1903–1908. [PubMed: 9257855]

13. Gazzinelli R, Xu Y, Hieny S, Cheever A, Sher A. Simultaneous depletion of CD4+ and CD8+ T lymphocytes is required to reactivate chronic infection with Toxoplasma gondii. J Immunol. 1992; 149:175–180. [PubMed: 1351500]

14. Suzuki Y, Orellana MA, Schreiber RD, Remington JS. Interferon-gamma: the major mediator of resistance against Toxoplasma gondii. Science. 1988; 240:516–518. [PubMed: 3128869]

15. Sallusto F, Geginat J, Lanzavecchia A. Central memory and effector memory T cell subsets: function, generation, and maintenance. Annu Rev Immunol. 2004; 22:745–763. [PubMed: 15032595]

16. Sallusto F, Lanzavecchia A, Mackay CR. Chemokines and chemokine receptors in T-cell priming and Th1/Th2-mediated responses. Immunol Today. 1998; 19:568–574. [PubMed: 9864948]

17. Strack A, Schluter D, Asensio VC, Campbell IL, Deckert M. Regulation of the kinetics of intracerebral chemokine gene expression in murine Toxoplasma encephalitis: impact of host genetic factors. Glia. 2002; 40:372–377. [PubMed: 12420316]

18. Khan IA, et al. IP-10 is critical for effector T cell trafficking and host survival in Toxoplasma gondii infection. Immunity. 2000; 12:483–494. [PubMed: 10843381]

19. Wilson EH, et al. Behavior of parasite-specific effector CD8+ T cells in the brain and visualization of a kinesis-associated system of reticular fibers. Immunity. 2009; 30:300–311. doi:10.1016/j.immuni.2008.12.013. [PubMed: 19167248]

20. Cahalan MD, Parker I. Choreography of cell motility and interaction dynamics imaged by two-photon microscopy in lymphoid organs. Annu Rev Immunol. 2008; 26:585–626. [PubMed: 18173372]

21. Miller MJ, Wei SH, Parker I, Cahalan MD. Two-photon imaging of lymphocyte motility and antigen response in intact lymph node. Science. 2002; 296:1869–1873. doi:10.1126/science.1070051. [PubMed: 12016203]

22. Zumofen G, Klafter J. Laminar-localized-phase coexistence in dynamical systems. Phys Rev E Stat Phys Plasmas Fluids Relat Interdiscip Topics. 1995; 51:1818–1821. [PubMed: 9962838]

23. Newman MEJ. Power laws, Pareto distributions and Zipf's law. Contemporary Physics. 2005; 46:323–351.

24. Johnson JB, Omland KS. Model selection in ecology and evolution. Trends Ecol Evol. 2004; 19:101–108. doi:10.1016/j.tree.2003.10.013. [PubMed: 16701236]

25. Potdar AA, Lu J, Jeon J, Weaver AM, Cummings PT. Bimodal analysis of mammary epithelial cell migration in two dimensions. Ann Biomed Eng. 2009; 37:230–245. doi:10.1007/s10439-008-9592-y. [PubMed: 18982450]

26. Budhu S, et al. CD8+ T cell concentration determines their efficiency in killing cognate antigen-expressing syngeneic mammalian cells in vitro and in mouse tissues. The Journal of experimental medicine. 2010; 207:223–235. doi:10.1084/jem.20091279. [PubMed: 20065066]

27. Li Y, Karlin A, Loike JD, Silverstein SC. Determination of the critical concentration of neutrophils required to block bacterial growth in tissues. The Journal of experimental medicine. 2004; 200:613–622. doi:10.1084/jem.20040725. [PubMed: 15353554]

28. Viswanathan GM, et al. Optimizing the success of random searches. Nature. 1999; 401:911–914. doi:10.1038/44831. [PubMed: 10553906]

29. Reynolds AM, Bartumeus F. Optimising the success of random destructive searches: Levy walks can outperform ballistic motions. J Theor Biol. 2009; 260:98–103. doi:10.1016/j.jtbi.2009.05.033. [PubMed: 19501601]

30. Sims DW, Righton D, Pitchford JW. Minimizing errors in identifying Levy flight behaviour of organisms. J Anim Ecol. 2007; 76:222–229. doi:10.1111/j.1365-2656.2006.01208.x. [PubMed: 17302829]

31. Pepper M, Dzierszinski F, Crawford A, Hunter CA, Roos D. Development of a system to study CD4+-T-cell responses to transgenic ovalbumin-expressing Toxoplasma gondii during toxoplasmosis. Infect Immun. 2004; 72:7240–7246. [PubMed: 15557649]

32. Dzierszinski F, et al. Presentation of Toxoplasma gondii antigens via the endogenous major histocompatibility complex class I pathway in nonprofessional and professional antigen-presenting cells. Infect Immun. 2007; 75:5200–5209. [PubMed: 17846116]

33. Wilson EH, Wille-Reece U, Dzierszinski F, Hunter CA. A critical role for IL-10 in limiting inflammation during toxoplasmic encephalitis. Journal of neuroimmunology. 2005; 165:63–74. doi:10.1016/j.jneuroim.2005.04.018. [PubMed: 16005735]
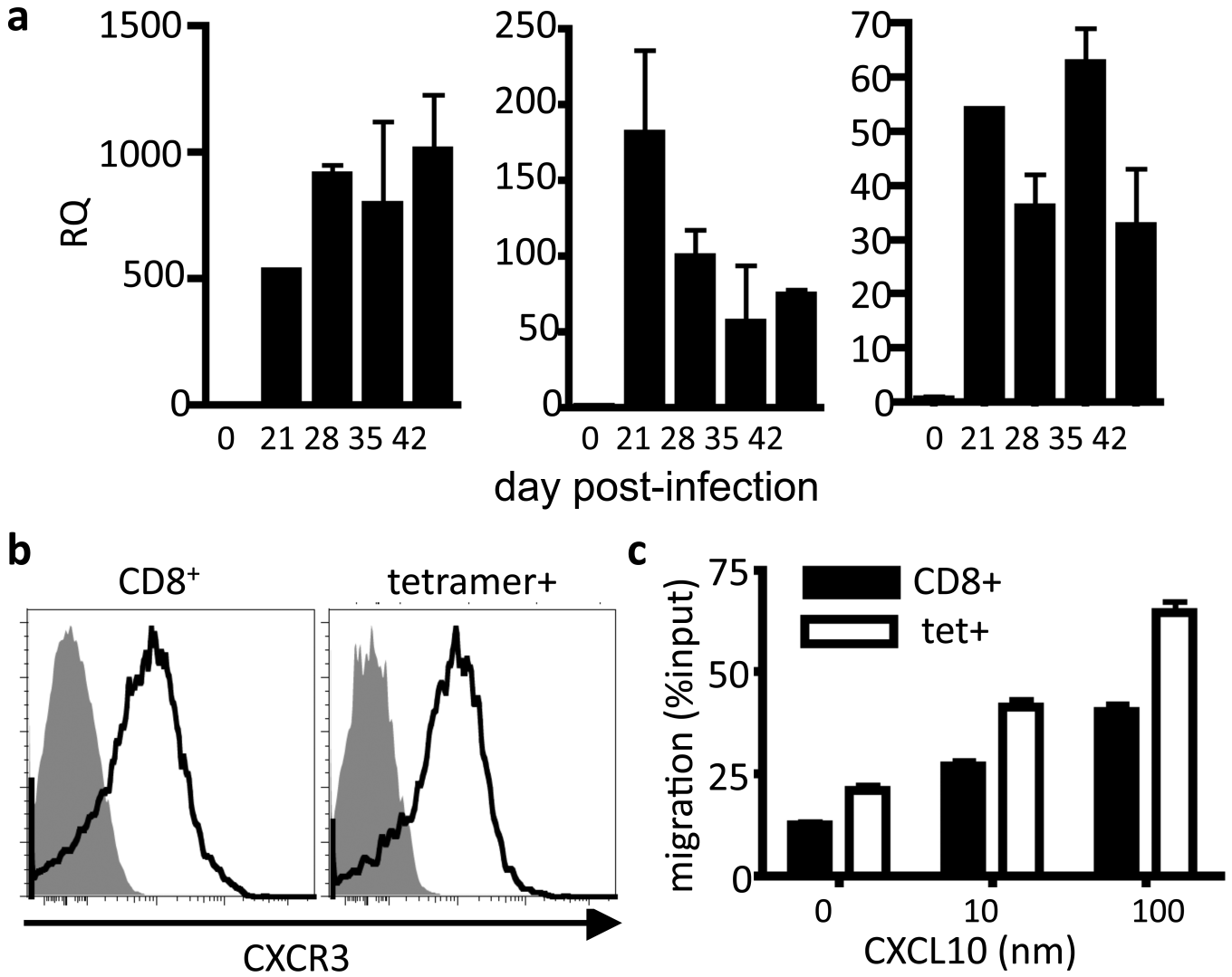
a

b

CD8⁺ tetramer+

CXCR3

c

■ CD8+
□ tet+

Figure 1. Chemokine and chemokine receptor expression in the brain during chronic toxoplasmosis

C57BL/6 mice were infected and RNA was isolated from whole brain tissue. Real time PCR specific for *cxcl9*, *cxcl10*, and *cxcr3* was performed and normalized to *hprt* mRNA. Results are depicted mean ± s.e.m. of fold increase over uninfected brain. Data is representative of two independent experiments with three mice per group (**a**). **c-d**, Brain mononuclear cells (BMNC) were purified on day 35 post-infection. CXCR3 expression (solid line, mean ± s.e.m.) by CD8⁺ and K^b-SIINFEKL⁺ (tet⁺) cells was measured by flow cytometry (**c**). The gray histogram represents the FMO control. Data is representative of three independent experiments. Purified BMNC were used in *ex vivo* chemotaxis assays. The mean ± s.e.m. percentage of cells that migrated toward CXCL10 are depicted (**d**). Results are representative of three independent experiments, n=3.
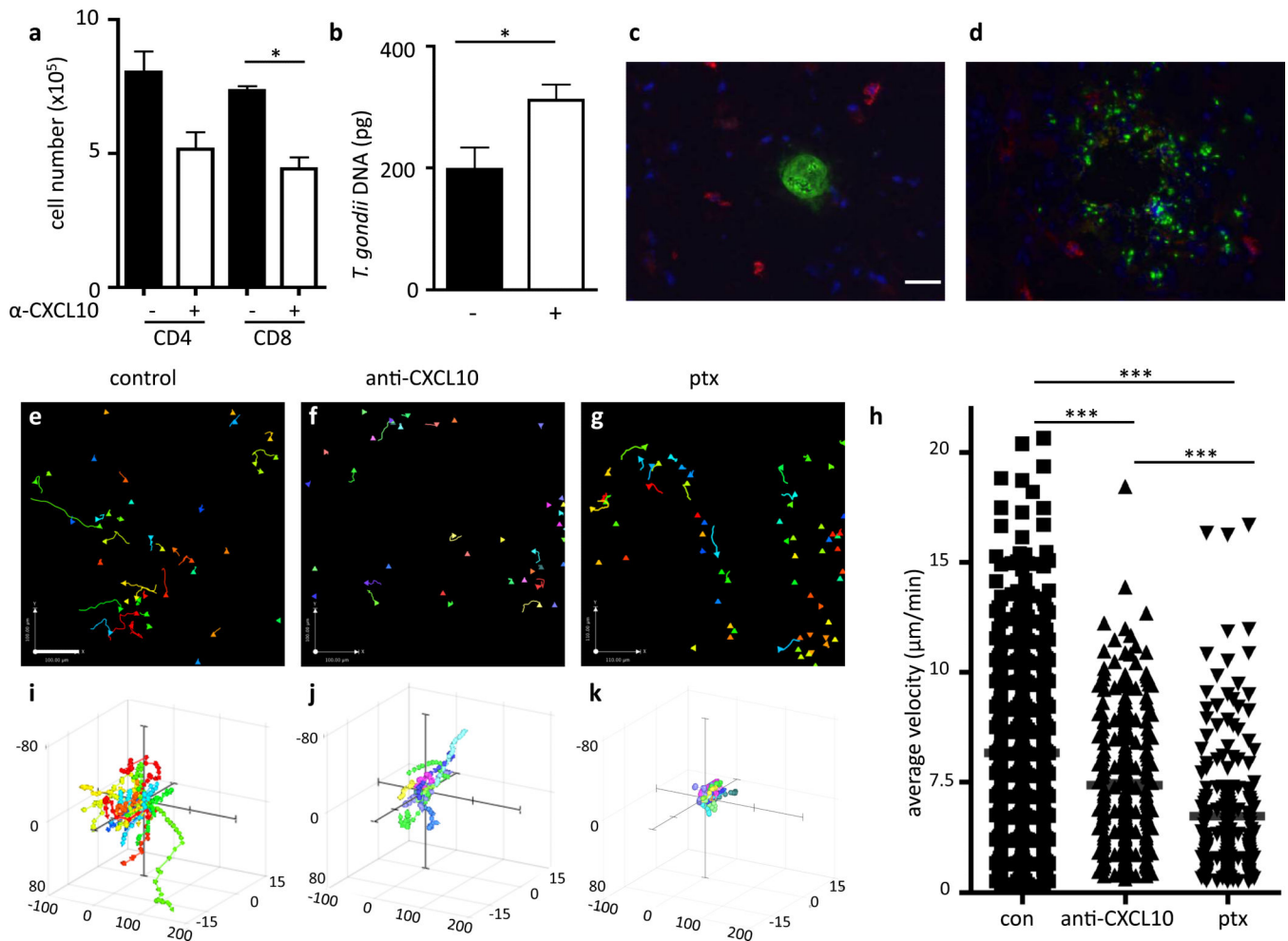
Figure 2. CXCL10 affects the CD8^{+} T cell population and the control of parasite replication
a-b, Mice chronically infected with Pru[OVA] were treated with anti-CXCL10 (+) antibody or control antibody (-). T cells isolated from the brain were identified by flow cytometry (**a**). Parasite burden was measured in the brain using real time PCR (**b**). Results are depicted as mean ± s.e.m. of three independent experiments, n=3-4 per group. *p 0.05, paired student's t-test. **c-d,** Immunohistochemical staining of brain sections for *T. gondii* (green), CD8 (red), and DAPI (blue) in anti-CXCL10-treated mice (**c**) and control animals (**d**). Size bar = 20μm. OTI[GFP] cells were expanded *in vitro* and transferred to mice chronically infected with Pru[OVA] parasites. On day 7 post-transfer, brains from mice that received PBS (con), 300 μg of anti-CXCL10 (anti-CXCL10), or 8 μg pertussis toxin (ptx) i.p. were imaged in 3 dimensions over 10 minutes. Representative cells tracks from control (**e**), anti-CXCL10 (**f**), and pertussis-toxin-treated mice (**g**) are shown (size bars, 100 μm). Volocity software was used to calculate the average track velocity (the average over all cells of the total displacement divided by the total observation time) (**h**). Cell motility was visualized by plotting individual cell tracks from the origin from control (**i**), anti-CXCL10-treated (**j**), and pertussis-toxin-treated (**k**) mice. **p<0.01, ***p<0.001 by one way ANOVA. Cell track data was obtained from three independent experiments with two mice per group. Control, 12 movies, n=507 cells; anti-CXCL10, 10 movies, n=280 cells; and ptx, 7 movies, n=192 cells.
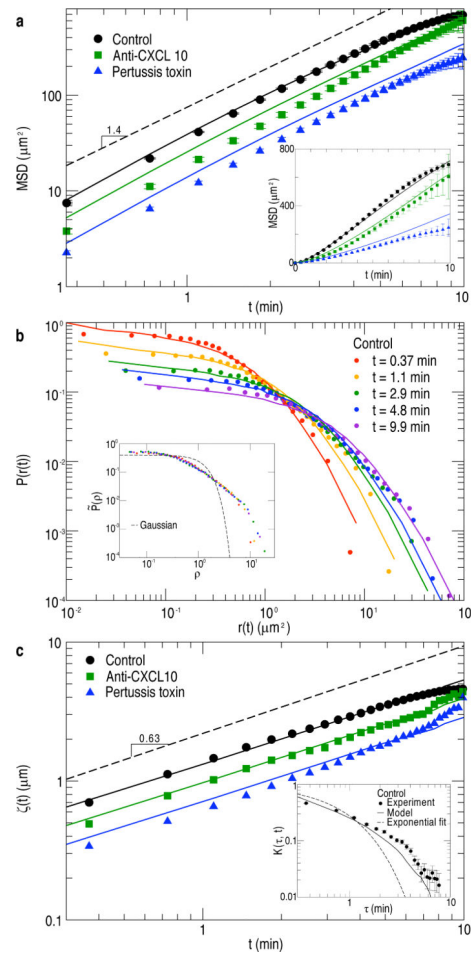
Figure 3. CD8⁺ T cell migration tracks are consistent with generalized Lévy walks
We compare experimental data for cells in control (black circles), anti-CXCL10-treated (green squares), and pertussis toxin-treated (blue triangles) mice with results for the generalized Lévy walk model (solid lines). (**a**) The mean squared displacement (MSD) grows nonlinearly in time, scaling approximately as t^{α}, where $\alpha \approx 1.4$ (dashed line). **Inset**: Linear plot of the MSD. Error bars depict s.e.m. (**b**) The probability distributions, $P\left(\overrightarrow{r}(t)\right)$, of T cell displacements at several different times, t, as indicated in the legend, for cells from control mice only. In order to avoid artifacts[30], histograms were constructed by placing 2500, 2000, 1500, 1300, or 600 displacements in each bin for t=0.37 min, 1.1 min, 2.9 min, 4.8 min, or 9.9 min, respectively. **Inset**: The displacement probability distributions at different times t collapse onto a single curve when the displacement is scaled by $\zeta(t)$. For comparison, a scaled Gaussian distribution is displayed (dashed line). (**c**) The scale factor, $\zeta(t)$, used to rescale displacements in (**b**) increases approximately as a power law, t, where $\gamma \approx 0.63$. **Inset**: Normalized displacement correlations, $\langle K(\tau,t)\rangle = \langle r(0,t) \cdot r(\tau,\tau+t)\rangle / \langle r^2(0,0)\rangle$, for control cells decay more slowly than exponentially (dashed line) with time τ.
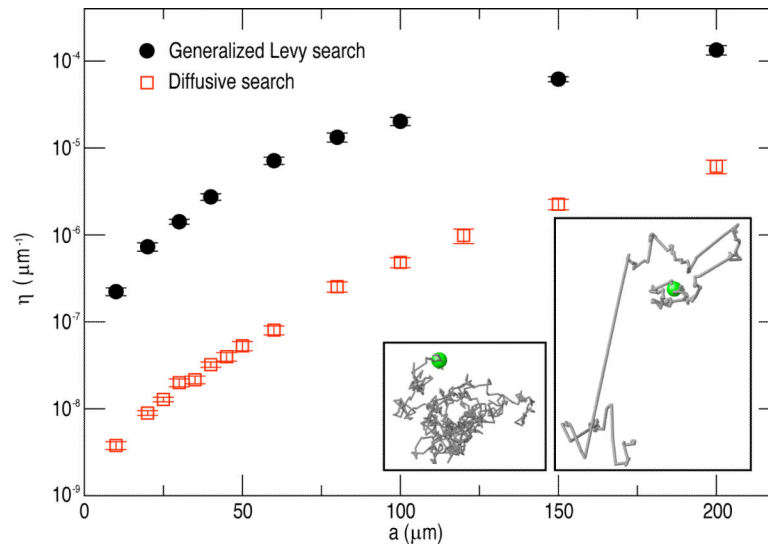
Figure 4. Generalized Lévy walks find targets more efficiently than random walks
We determined efficiency for generalized Lévy walkers (black circles) and Brownian walkers (open red squares) as a function of the target radius, *a*. The generalized Lévy search is considerably more efficient, especially when the targets are small. Error bars are the s.e.m. Examples of trajectories for Brownian walks (small inset) and the generalized Lévy walk model (large inset) are shown.